Integration of ZnO Nanotubes with Well-Ordered Nanorods through Two-Step Thermal Evaporation Approach

D. H. Fan, W. Z. Shen,* M. J. Zheng, Y. F. Zhu, and J. J. Lu

Laboratory of Condensed Matter Spectroscopy and Opto-Electronic Physics, Department of Physics, Shanghai Jiao Tong University, 1954 Hua Shan Road, Shanghai 200030, People's Republic of China

We have successfully realized the integration of ZnO nanotubes and well-ordered nanorods through a simple two-step thermal evaporation of Zn powder without any metal catalyst. Detailed structural analysis shows that the step-one prepared samples at the low substrate temperature are composed of hexagonal-shaped Zn/Zn suboxide nanowires dominated by Zn with little oxidation via the layer-by-layer growth mechanism. In the second step, by heating the step-one deposited samples and Zn powder at high temperature, highly ordered single-crystalline ZnO nanorods were epitaxially grown on the surface of nanowires through the screw dislocation growth mode. Simultaneously, Zn inside the nanowires sublimates to form hollow ZnO nanotubes, which finally results in the formation of ZnO nanotubes surrounded by well-ordered nanorods (ZNSWN). The field-emission scanning electron microscopy images of samples with different heating times indicate that the length of ZnO nanorods in the tube walls can be well controlled by changing the reaction time with a growth rate of ~3 nm/min. We also further present the comparative X-ray diffraction, Raman, and photoluminescence investigation for the growth process and structural information of the fabricated ZNSWN nanostructures.

I. Introduction

Zinc oxide (ZnO) is an important wide band gap (3.37 eV) semiconductor with interesting piezoelectric, pyroelectric, photoconducting properties, and a large exciton binding energy of 60 meV at room temperature. Structurally, the alternatively stacking of zinc and oxygen atoms along the *c*-axis induces two polar surfaces in ZnO, that is, positively charged (0001)-Zn and negatively charged (000$\bar{1}$)-O, besides, ZnO has three fast growth directions of [0001], [10$\bar{1}$0], and [2$\bar{1}$$\bar{1}$0].[1,2] These unique structural properties have benefited the realization of many kinds of novel ZnO nanostructures, including nanobelts,[2] nanorings,[3] nanoprisms,[4] nanowires,[5] nanobridges,[6] nanonails,[6] nanopropellers,[7] nanowhiskers,[8] nanotubes,[9] and nanopores.[10] The variety of ZnO nanostructures has provided strong potential in the application of nanoscale devices. One-dimensional (1-D) ZnO nanostructures have been demonstrated in the nanolasings,[11] nanoresonators,[12] photonic crystals,[13] photodetectcors,[14] optical modulator waveguides,[15] light-emitting diodes,[16] field emitters,[17] gas sensors,[18] solar cells,[19] and so on. However, the characteristics of the nanodevices depend significantly on the shape and size of the nanostructures. Fabricating hierarchical 1-D ZnO nanostructures in a controllable manner is required to improve the performance and to broaden the application, but one still faces remarkable challenges.
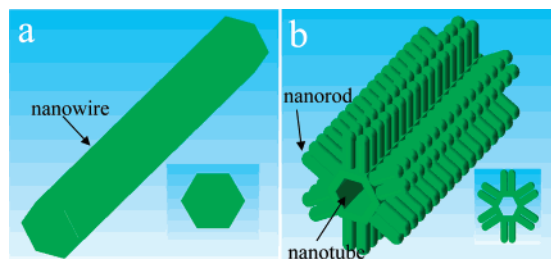
In this paper, we report the controllable growth of novel hierarchical nanostructures, that is, ZnO nanotubes surrounded by well-ordered nanorods (ZNSWN), through a simple two-step thermal evaporation deposition approach. The successful integration of the hierarchical 1-D ZnO nanostructures takes advantage of two different stages with the substrate temperature below and above the melting point of Zn (419.5 °C), along with

the consideration of polar surfaces and fast growth directions of hexagonal ZnO. Figure 1 displays the formation process of the ZNSWN schematically. We first synthesized the hexagonal-shaped Zn/Zn suboxide nanowires (Figure 1a) at a low substrate temperature of ~200 °C by evaporating Zn powder. With continuous supplementation of Zn and Zn suboxide gases at 500 °C in the second step, highly ordered ZnO nanorods were epitaxially grown on the surface of the nanowires because of the screw dislocation growth mechanism. At the same time, the Zn inside the nanowires was sublimated, while the Zn on the nanowires' sidewall was oxidized, enabling the transformation from Zn nanowires to hollow ZnO nanotubes. The simultaneous growth of ZnO nanorods and the formation of nanotubes led to the realization of ZNSWN nanostructures (Figure 1b). The length of the nanorods could also be well controlled via changing the evaporation time. Our present method provides the possibility of a general approach for nanounit integration and paves the way for the realization of hierarchical 1-D ZnO nanostructures in novel nanodevice applications.

II. Experimental Details

The hierarchical ZnO nanostructures were synthesized in a horizontal tube furnace system by a two-step thermal vapor deposition process. In the first step, pure zinc powder (99.99%) of 0.6 g was placed in an alumina boat located at the center of a horizontal quartz tube. N-type Si wafer cleaned by sonication in ethanol and acetone was employed as the substrate and was placed at the downstream position of the carrier gas. The quartz tube was evacuated to ~2.0 Pa using a mechanical rotary pump to remove the residual oxygen before heating. When the source material was heated to 500 °C at a rate of 10 °C/min, pure (99.9%) argon and oxygen were used as the carrier gas and were introduced from one end of the quartz tube at a flow rate of 300 standard cubic centimeters per minute (sccm) and 80

* To whom correspondence should be addressed. Fax: +86-21-54743242. E-mail: wzshen@sjtu.edu.cn.

Integration of ZnO Nanotubes with Nanorods

J. Phys. Chem. C, Vol. 111, No. 26, 2007 **9117**

Figure 1. Schematic diagrams of the growth process for the nanostructure of ZNSWN. (a) Zn/Zn suboxide nanowire prepared in step-one thermal evaporation. (b) ZNSWN nanostructure fabricated by two-step thermal evaporation approach. The insets in a and b show the cross section of the corresponding nanowire and ZNSWN nanostructure.

sccm, respectively. During evaporation, the measured substrate temperature was around 200 °C. The detailed growth conditions of the step-one prepared samples (namely, sample nos. 1−3) have been listed in Table 1. After heating, the tube was cooled naturally to room temperature under the above-mentioned atmosphere, and gray products were found covering the silicon substrate.

In the second step, sample no. 1 was used as the substrate to prepare ZNSWN structure, and it was placed along the downstream side of the carrier gas. Argon and oxygen were still used as the carrier gas at a flow rate of 260 and 60 sccm, respectively. We put the sample 2 cm away from the Zn source horizontally and prepared sample nos. 4−6 with the Zn source heating (varied time span from 80 to 20 min) at 500 °C, and the substrate temperature was also monitored during the growing process at around 500 °C. We also prepared sample no. 7 without Zn source for comparison. The detailed growth conditions of these samples have also been listed in Table 1. Finally, when the reaction was over, the quartz tube was cooled naturally to room temperature and the color of the substrate's surface turned from gray to gray-white.

The morphology and structure of the samples were characterized using the field-emission scanning electron microscopy (FESEM) (Philips XL30FEG), the high-resolution transmission electron microscope (HRTEM) (JEOL JEM-2100F), and X-ray diffraction (XRD) (Bruker D8 ADVANCE system with Cu Kα of 1.5406 Å). Raman and photoluminescence (PL) spectra were recorded at room temperature by a Jobin Yvon LabRAM HR 800UV micro-Raman/PL system under an Ar$^+$ (514.5 nm) and He−Cd (325.0 nm) laser excitation, respectively.

III. Results and Discussion

Figure 2a shows the FESEM image of the prepared sample no. 1. It exhibits hexagonal-shaped nanowires with widths of 300−600 nm and lengths up to several-decade micrometers. High-magnification image of Figure 2b displays flat and smooth terracelike and steplike structures on the hexagonal-shaped ends,

clearly revealing a layer-by-layer growth mode. This is consistent with the previous report on the ZnO nanorod prepared by the metalorganic vapor-phase epitaxy.[20] There are not any nanoparticles at the end of nanowires, suggesting that the growth mechanism is not vapor−liquid−solid (VLS) process because a typical characteristic of VLS is the existence of nanoclusters capping at the end of a 1-D nanostructure.[21,22] Apart from the Zn and O element, no other elements are observed in the energy-dispersive X-ray (EDX) spectrum of Figure 2c, which confirms that there is no existence of other metal clusters in the Zn/Zn suboxide nanowires and also excludes the possibility that the nanowires are realized by the catalysis-assisted growth. The relatively large atomic ratio of Zn and O (∼19:1) indicates that little Zn is oxidized into Zn suboxide at the first step, that is, the nanowire is dominated by Zn with little oxidation.

To further understand the growth mechanism of Zn/Zn suboxide nanowire, we present in Figure 2d and 2e the low- and high-magnification SEM images of sample no. 2. The deposition time of sample no. 2 is only 7 min, which stands for the early growth stage of the nanowire. It is found that nanocrystals with hexagonal morphology have been formed on Si substrate with different widths, and the fact that a smaller sheet lies on the larger one implies that the formation of long nanowires in Figure 2a should originate from the absorption of Zn/Zn suboxide at the initial nanocrystal tips.

Furthermore, the introduction of the flowing carrier gas also plays an important role in the formation of nanowires. Figure 2f gives the SEM morphology of sample no. 3 prepared in the vacuum, where many clusters of zinc are synthesized on Si substrate with few nanowires formed. Laminar gas flow may induce turbulence in a certain growth condition, which results in the adsorption of fresh reactant gases on nanowire tips with more surface steps. Consequently, the growth rate of nanowire tips is higher than that on sidewalls, which effectively promotes the growth of nanowires.

According to the above experimental observation, we can deduce the following growth mechanism. In the heating process, Zn vapor is formed by evaporating Zn powder with little Zn oxidized into Zn suboxide because of the limited oxygen content. Zn and Zn suboxide are transported to the low-temperature region by the carrier gas and are absorbed on the surface of the Si substrate. Since Zn belongs to the hexagonal crystal system with the sixfold symmetry, Zn and Zn suboxide atoms on the substrate could migrate and form the steady hexagonal nanostructure.

The hexagonal moundlike morphology in Figure 2d and 2e indicates the existence of an Ehrlich−Schwoebel barrier (ESB) during the formation of Zn/Zn suboxide nanowires.[4,23] During the formation process of 1-D nanostructure, if the adspecies on the nucleated island experience an ESB when diffusing across the island's edge, the next atomic layer may nucleate before

TABLE 1: Detailed Experimental Conditions for the Seven Samples

samples	method	Ar flow rate (sccm)	O flow rate (sccm)	work pressure (Pa)	substrate and Zn powder distance (cm)	measured substrate temperature (°C)	heating time (min)	existence of Zn source (yes or no)	substrate
no. 1	one step	300	80	180	34	∼200	60	yes	Si
no. 2		300	80	180	34	∼200	7	yes	Si
no. 3		300	80	vacuum	34	∼200	60	yes	Si
no. 4	two step^a	260	60	180	2	∼500	80	yes	no. 1
no. 5		260	60	180	2	∼500	50	yes	no. 1
no. 6		260	60	180	2	∼500	20	yes	no. 1
no. 7		260	60	180	no	∼500	80	no	no. 1

^{a} Sample no. 1 prepared at the first step is used as the substrate at the second step.
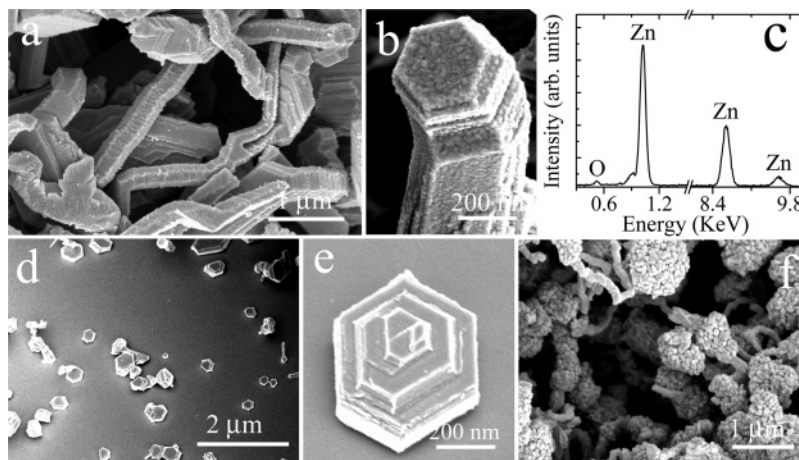
Figure 2. (a) Low- and (b) high-magnification SEM images of hexagonal-shaped Zn/Zn suboxide nanowires (sample no. 1) formed in the first step (60 min). (c) EDX spectrum of Zn/Zn suboxide nanowires. (d) Low- and (e) high-magnification SEM images of sample no. 2 deposited for only 7 min in the first step. (f) SEM image of sample no. 3 prepared in the vacuum condition.
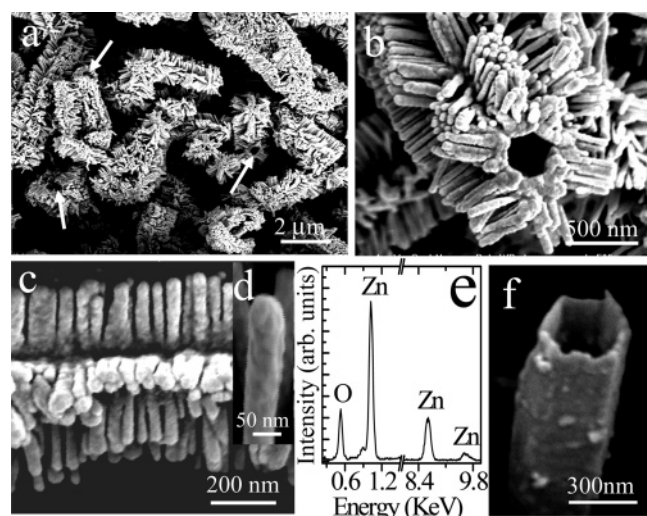
Figure 3. (a) Low- and (b) high-magnification SEM images of the prepared ZNSWN nanostructure (sample no. 4) through the two-step thermal evaporation approach. (c) SEM image of nanorods on the nanotube sidewall and (inset, d) high-magnification SEM image of a single nanorod. (e) EDX spectrum of the ZNSWN nanostructure. (f) SEM image of the prepared nanotube without Zn source in the second step.

the previous layer completes, thereby leading to the multilayer growth and the eventual appearance of the mound structure. Baxter et al.[24] have shown that the ESB plays an essential role in the formation of ZnO hexagonal pyramids. However, the ESB decreases with the increase of heating time in the evaporation, resulting in the relatively smoother surface in Figure 2a and 2b as compared with that in Figure 2d and 2e. Similar observation has been reported by Liu et al.[4] in nanoprisms, where the next atomic layer would not nucleate until the previous one has completed because of the very small ESB in the layer-by-layer growth mode.

The novel hierarchical 1-D ZnO nanostructures can be yielded by evaporating the Zn powder at 500 °C and by heating the Zn/Zn suboxide nanowires simultaneously at the same temperature. Figure 3a shows the SEM image of sample no. 4 after the second step, which displays an interesting nanostructure of ZNSWN. The arrows in the figure indicate the open tips of the ZnO nanotubes, clearly revealing the tubular nanostructures with length of several decade micrometers and inner diameter of 200−500 nm. The high-magnification SEM image in Figure 3b presents the detailed morphology of ZNSWN, exhibiting that

the nanotubes have hexagonal cross sections with well-ordered nanorods formed on its six sidewalls. Figure 3c shows the image of nanorods on the nanotube sidewall with widths of 30−100 nm and lengths of around 250 nm. The high-magnification image of a single nanorod in Figure 3d reveals a columniform structure with a conic tip, which is quite different from the hexagonal structure formed at the first step in Figure 2b, indicating that the ZnO nanorods are not synthesized through the layer-by-layer growth mechanism.[20] By comparing the EDX spectrum of sample no. 4 (Figure 3e) with sample no. 1 (Figure 2c), although no other new elements have been introduced except Zn and O, the atomic ratio of Zn and O decreases to 1.05:1, which demonstrates that Zn has almost been oxidized at the second stage.

The origins of the nanorods should be further investigated by designed experiments. Figure 3f shows the SEM image of sample no.7 synthesized without the Zn source, which demonstrates clearly the absence of nanorods on the surface of the nanotubes, indicating that the existence of Zn source is responsible for the formation of nanorods in ZNSWN nanostructures, while the sublimed Zn is not. In addition, we can observe that the sidewall thickness of the nanotubes has increased, which reveals the diameter increase of the nanowires. As there is a thin layer of ZnO on the surface of the nanowires (step one), the surface of nanowires will not be sublimed because of the high melting point (1975 °C) of ZnO. It also indicates that before the growth of the nanorods on the sidewall in the beginning of the second step, Zn and Zn suboxide gas will first nucleate and form the ZnO layer on the surface of nanowires, resulting in the increase of the physical diameter during the transformation of nanowires to nanotubes structure. Furthermore, it should be clarified for the motivation of introducing an appropriate amount of oxygen in argon gas flow in step one, which is helpful for the realization of ZNSWN nanostructures. On the one hand, it will help to form a thin ZnO film on the sidewall of the Zn nanowires, which is the base for the later growing of ZnO nanorods; on the other hand, if pure argon is used in the experiment, we will see the forming of pure Zn nanowires, but when it comes to the next deposition stage, the surface of the pure Zn nanowires will be oxidized and sublimed simultaneously, so that the surface oxidation will be uneven, which is detrimental for the realization of high-quality ZNSWN nanostructure.

Further morphological and structural analysis of individual ZNSWN nanostructure can be characterized by the HRTEM

Integration of ZnO Nanotubes with Nanorods

J. Phys. Chem. C, Vol. 111, No. 26, 2007 **9119**
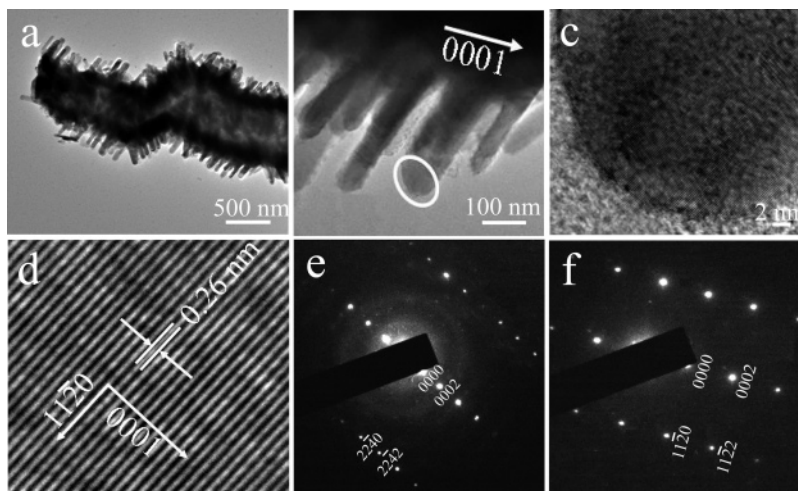
Figure 4. TEM and HRTEM images of the ZNSWN nanostructure sample no. 4. (a) TEM image of a single ZNSWN nanostructure. (b) TEM image of nanorods on the surface of a single nanotube. (c) HRTEM image of a nanotip indicated by the ellipse in b. (d) HRTEM image and (e) the corresponding SAED pattern of the nanorods. (f) SAED pattern of the tube wall conjoint with nanorods.

and selected area electron diffraction (SAED). Figure 4a shows the TEM morphology of the ZNSWN sample no. 4, which consists of the nanotube with the light inner part and relatively dark outer one, together with the nanorods on the surface of the outer wall. The result further confirms that the prepared nanostructures belong to the hierarchical ZNSWN nanostructures. The high-magnification image of the sidewall in Figure 4b reveals that the length of the nanorods is around 250 nm and the width is around 30−100 nm. Figure 4c displays the HRTEM profile image of a nanotip on the nanorod (indicated by the ellipse in Figure 4b), clearly demonstrating that no nanocluster or tiny nanocrystal is formed at the growth front. The lattice fringes of ZnO nanorods in Figure 4d and the corresponding SAED pattern in Figure 4e indicate that the nanorod is single crystalline, and it grows along [11$\bar{2}$0] direction with a uniform structure without noticeable defects such as stacking faults. The lattice spacing of 0.26 nm corresponds to the spacing of [0002] crystal planes of wurtzite ZnO. Figure 4f shows that the SAED pattern of the tube wall is conjoint with nanorods, which indicates that the nanotube is also single crystalline with growth direction along [0001]. In the idealized ZnO crystal growth, 1-D ZnO nanostructures generally grow along [0001] direction because of the high growth rate along this orientation compared with the others.[8] However, considering the fact that the side face on the ZnO nanotube is along the {11$\bar{2}$0} direction, one can expect the [11$\bar{2}$0] growth of the nanorod because of the restriction of the epitaxial relationship, that is, the growth direction of the nanorod is determined by that of the nanotube wall. Similar experimental observation has been previously reported by Fan et al.[25]

Generally speaking, the oxidation rate varies with the crystal surfaces. In comparison with other surfaces, the Zn{0001} one has the lowest energy, which tends to be the most stable to resist oxidation.[26] When the Zn/Zn suboxide nanowires are heated at ∼500 °C, the sidewall of hexagonal nanowires is oxidized into ZnO shells since the {11$\bar{2}$0} surface has the relatively higher energy compared with the {0001} one. At the same time, the remaining Zn inside the nanowires can be sublimed through the open ends at the {0001} surface because of the low melting point of Zn (419.5 °C), leading to the formation of hexagonal ZnO nanotubes. The growth direction of nanotubes in Figure 4b and 4f confirms our arguments.

Apart from the VLS mechanism, the screw dislocation mechanism is also well acknowledged to explain the growth

dynamics of 1-D nanomaterial.[21] From Figures 3d and 4c, it is clear that no additional metal particles or tiny nanocrystals appear on the top of the nanorods, ruling out the possibility of the catalysis process during the growth of well-aligned ZnO nanorods.[21,22,27] On the other hand, the growth rate along the dislocation line in the screw dislocation model is much higher than that along the radius direction, resulting in the crystal 1-D structure morphology.[21,28,29] The conic tip with spiral morphology at the end of 1-D structured materials is the evidence that screw dislocation mechanism manifests itself. From the SEM and TEM image of non-hexagonal-shaped nanorods in Figures 3 and 4, our observation agrees well with the characteristics of smooth facets and rough tips in the screw dislocation growth model.

We can therefore conclude the formation process of ZNSWN from the above observations and arguments. Zn and Zn suboxide gases yielded by heating Zn powder are transported to the substrate and nucleate at the Zn/Zn suboxide nanowires. During the second step of the growing process, the yielded Zn and Zn suboxide gases first nucleate on the surface of the nanowires and form the ZnO layer. With continuous supplementation of Zn and Zn suboxide gases, the ZnO nanorods are epitaxially grown on the surface of the nanowires because of the screw dislocation growth mechanism. At the same time, the hexagonal ZnO nanotubes are gradually formed because of the sublimation of the remaining Zn inside the nanowires. With the further increase of the evaporation time, the ZNSWN nanostructure is then realized. In addition, the different nucleation dimensions on the nanotube side facet may result in the observed nonuniform width (30−100 nm) of the nanorods.

To make the growth of nanorods controllable, we carried out a set of experiments by varying heating time on the Zn/Zn suboxide nanowires. Figure 5a−c shows the SEM images of the ZNSWN samples prepared at 20, 50, and 80 min, respectively, in the step-two stage. It is clear that, with the increase of reaction time, the length of nanorods increases from ∼50 to 250 nm, demonstrating the nucleation, absorption, and growth process, which as a whole increases the length of nanorods. The variation of nanorods in Figure 5 suggests that we can control the length of nanorods by adjusting the reaction time (growth rate of ∼3 nm/min) with the nanotubes' hexagonal cross sections remaining unchanged.

In addition to the above ordinary morphological means of observations, structural and optical characterizations including
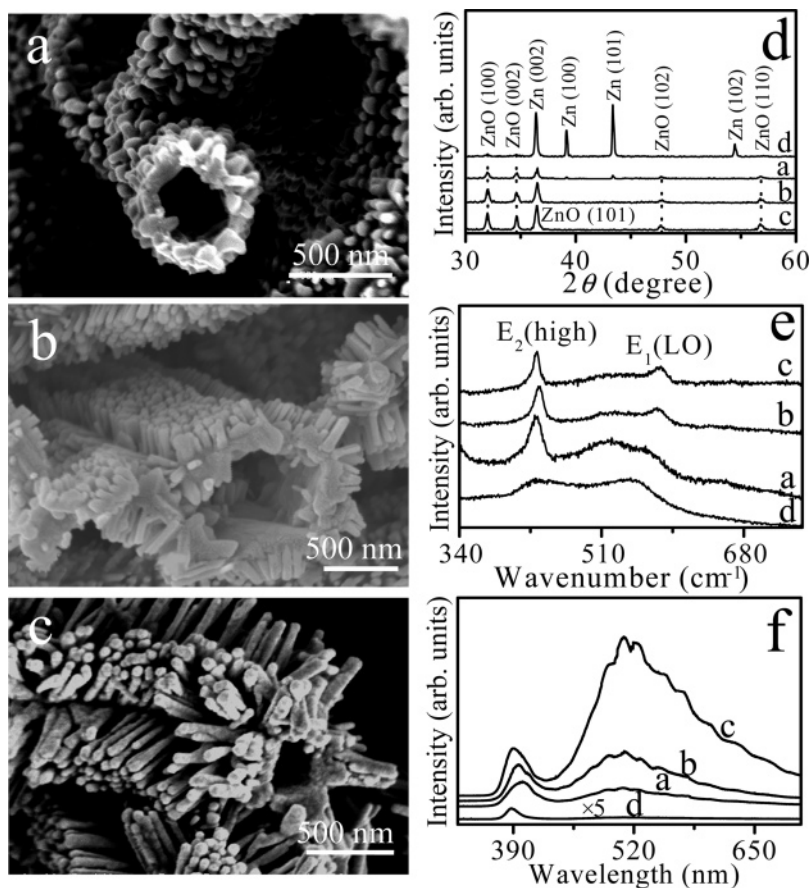
Figure 5. SEM images of ZNSWN samples prepared for different heating times: (a) 20 min (sample no. 6), (b) 50 min (sample no. 5), and (c) 80 min (sample no. 4). (d) XRD, (e) Raman, and (f) PL spectra of the three ZNSWN nanostructures (curve a: 20 min, b: 50 min, and c: 80 min) together with those of the step-one prepared sample no. 1 (curve d) for comparison.

XRD, Raman, and PL spectra could provide different perspectives to gain more insight into the growth process and structural information of the fabricated ZNSWN nanostructures. Figure 5d shows the XRD spectra of the hierarchical ZNSWN samples under different heating times (curve a, 20 min; b, 50 min; and c, 80 min) together with the Zn/Zn suboxide nanowires (curve d: sample no. 1) for comparison. It is found that sample no. 1 shows strong Zn (002), (100), (101), and (102) diffraction peaks with very weak ZnO (100), (002), and (101) structures,[9] which is in good agreement with the EDX result in Figure 2c. It also gives evidence of the thin layer of ZnO on the surface of the nanowires formed after step one, since the outer surface being exposed to the oxygen atmosphere is more likely to get oxidized. The Zn diffraction peaks dramatically decrease and finally disappear because of the increase of the ZnO structures after the samples are disposed in the second step. From Figure 5d, it also reveals that much Zn is oxidized into ZnO in ZNSWN sample no. 6 (curve a), while for sample nos. 5 and 4 (curves b and c), Zn is completely transformed into ZnO. Furthermore, the enhancement of ZnO (002) diffraction peak suggests that prolonging reaction time will lead to the improvement of the crystal quality of the synthesized ZNSWN nanostructures.

Figure 5e displays the Raman spectra of these samples. For sample no. 1 (curve d), a weak structure at 437 cm^{-1} corresponding to the E_2 mode of ZnO crystal indicates the existence of a small amount of ZnO,[30] and the ~550 cm^{-1} Raman peak is far from the two normal volume phonon vibration of perfect ZnO crystal, that is, two longitudinal acoustics (LA) mode of 538 cm^{-1} and E_1 (longitudinal optical: LO) mode of 584 cm^{-1}. Zeng et al.[31] have also observed similar results in the Zn/ZnO nanoparticles and believe that the ~550 cm^{-1} peak should be

surface optical phonon mode originating from the shell surface and grain boundaries and that the shift is due to the large distortion of interfacial atoms between Zn and ZnO. The gradual oxidation of Zn with the increase of heating time will change the Zn and ZnO interface, resulting in the blueshift of the Raman peak and line width narrowing of the E_2 (high) owing to the improvement of crystal quality (curves a–c). In addition, it is well accepted that the E_1 (LO) mode is thought to be associated with oxygen deficiency in samples.[32] The appearance of E_1 (LO) mode reveals the existence of defects in the ZNSWN samples.

The corresponding room-temperature PL spectra of these four samples are presented in Figure 5f. The luminescence intensity of the Zn/Zn suboxide nanowires (curve d) is very weak compared with that of the ZNSWN nanostructures because of the existence of little ZnO. There are mainly two peaks in the hierarchical ZNSWN samples with a weak ultraviolet (UV) emission at ~390 nm and a relatively strong green peak at ~510 nm. The UV peak could be generally attributed to the near-band-edge emission of the wide band gap ZnO, which originates from the recombination of free excitons. With the increase of heating time, the improvement of the crystal quality and the decrease of average nanoparticle size (as shown in Figure 5a–c) lead to the enhancement and blueshift of the UV peak.[33,34] Although no stacking fault is observed in the TEM image, we cannot rule out other types of defects in the ZNSWN samples because some defects such as vacancy or interstitial may not be visible during the HRTEM observation. The Raman spectra in Figure 5e have demonstrated the existence of oxygen deficiency. The green emission at ~510 nm in ZNSWN may originate from the transition between a singly ionized oxygen vacancy and a photogenerated hole.[35,36] It is well-known that

Integration of ZnO Nanotubes with Nanorods

J. Phys. Chem. C, Vol. 111, No. 26, 2007 **9121**

surface states play an important role in the PL characteristics of nanomaterials. Yao et al.[37] have suggested that the surface-to-volume ratio can influence the PL emission efficiency significantly. With the increase of nanorod length, the intensification of green emission (curves a–c) is closely related to the enhancement of the surface-to-volume ratio in ZNSWN.

IV. Conclusions

In summary, we have demonstrated the successful realization of hierarchical 1-D ZNSWN nanostructures through integrating ZnO nanotubes with nanorods by a simple two-step thermal evaporation approach. Detailed structural analysis reveals that the step-one prepared samples follow the layer-by-layer growth mechanism. They are composed of hexagonal-shaped Zn/Zn suboxide nanowires dominated by Zn with little oxidation because of the low substrate temperature of ~200 °C. Under the further supplementation of Zn and Zn suboxide gases at 500 °C in the second step, highly ordered single-crystalline ZnO nanorods are epitaxially grown from the nanowire surface through the screw dislocation growth mode, while Zn inside the nanowires sublimates to form the hollow ZnO nanotubes. The ZNSWN nanostructures are assembled because of the simultaneous formation of ZnO nanorods and nanotubes. Controllable length of nanorods has also been achieved by changing the reaction time with a growth rate of ~3 nm/min. We have further presented the comparative XRD, Raman, and PL investigation for the growth process and structural information of the fabricated ZNSWN nanostructures. In addition, this simple two-step thermal evaporation approach can integrate many kinds of single nanostructures into the hierarchical and controlled ones, which could greatly broaden the potential applications of nanostructures in novel nanodevices. For example, it is possible to fabricate hetero-nanostructures by assembling other materials such as In_2O_3 or CdO nanorods on ZnO nanotubes by evaporating In or Cd powder under suitable temperature at the second stage.

References and Notes

(1) Wang, Z. L.; Kong, X. Y.; Ding, Y.; Gao, P. X.; Hughes, W. L.; Yang, R.; Zhang, Y. *Adv. Funct. Mater.* **2004**, *14*, 943.
(2) Pan, Z. W.; Dai, Z. R.; Wang, Z. L. *Science* **2001**, *291*, 1947.
(3) Kong, X. Y.; Ding, Y.; Yang, R. S.; Wang, Z. L. *Science* **2004**, *303*, 1348.
(4) Liu, D. F.; Xiang, Y. J.; Zhang, Z. X.; Wang, J. X.; Gao, Y.; Song, L.; Liu, L. F.; Dou, X. Y.; Zhao, X. W.; Luo, S. D.; Wang, C. Y.; Zhou, W. Y.; Wang, G.; Xie, S. S. *Nanotechnology* **2005**, *16*, 2665.
(5) Zheng, M. J.; Zhang, L. D.; Li, G. H.; Shen, W. Z. *Chem. Phys. Lett.* **2002**, *363*, 123.
(6) Lao, J. Y.; Huang, J. Y.; Wang, D. Z.; Ren, Z. F. *Nano Lett.* **2003**, *3*, 235.
(7) Guo, P. X.; Wang, Z. L. *Appl. Phys. Lett.* **2003**, *84*, 2883.
(8) Hu, J. Q.; Bando, Y. *Appl. Phys. Lett.* **2003**, *82*, 1401.
(9) Hu, J. Q.; Li, Q.; Meng, X. M.; Lee, C. S.; Lee, S. T. *Chem. Mater.* **2003**, *15*, 305.
(10) Ding, G. Q.; Shen, W. Z.; Zheng, M. J.; Fan, D. H. *Appl. Phys. Lett.* **2006**, *88*, 103106.
(11) Huang, M. H.; Mao, S.; Feick, H.; Yan, H.; Wu, Y.; Kind, H.; Weber, E.; Russo, R.; Yang, P. *Science* **2001**, *292*, 1897.
(12) Bai, X. D.; Gao, P. X.; Wang, Z. L.; Wang, E. G. *Appl. Phys. Lett.* **2003**, *82*, 4806.
(13) Chen, Y.; Bagnall, D.; Yao, T. *Mater. Sci. Eng., B* **2000**, *75*, 190.
(14) Liang, S.; Sheng, H.; Liu, Y.; Huo, Z.; Lu, Y.; Shen, H. *J. Cryst. Growth* **2001**, *225*, 110.
(15) Lee, J. Y.; Choi, Y. S.; Kim, J. H.; Park, M. O.; Im, S. *Thin Solid Films* **2002**, *403*, 553.
(16) Saito, N.; Haneda, H.; Sekiguchi, T.; Ohashi, N.; Sakaguchi, I.; Koumoto, K. *Adv. Mater.* **2002**, *14*, 418.
(17) Li, Q. H.; Wang, Q.; Chen, Y. J.; Wang, T. H.; Jia, H. B.; Yu, D. P. *Appl. Phys. Lett.* **2004**, *85*, 636.
(18) Lin, Y.; Zhang, Z.; Tang, Z.; Yuan, F.; Li, J. *Adv. Mater. Opt. Electron.* **1999**, *9*, 205.
(19) Law, M.; Greene, L. E.; Johnson, J. C.; Saykally, R.; Yang, P. *Nat. Mater.* **2005**, *4*, 455.
(20) Park, W. I.; Kim, D. H.; Jung, S. W.; Yi, G. C. *Appl. Phys. Lett.* **2002**, *80*, 4232.
(21) Wu, J. J.; Liu, S. C. *J. Phys. Chem. B* **2002**, *106*, 9546.
(22) Shen, G. Z.; Bando, Y.; Liu, B. D.; Golberg, D.; Lee, C. J. *Adv. Funct. Mater.* **2006**, *16*, 410.
(23) Elliott, W. C.; Miceli, P. F.; Tse, T.; Stephens, P. W. *Phys. Rev. B* **1996**, *54*, 17938.
(24) Baxter, J. B.; Wu, F.; Aydil, E. S. *Appl. Phys. Lett.* **2003**, *83*, 3797.
(25) Fan, H. J.; Scholz, R.; Kolb, F. M.; Zacharias, M. *Appl. Phys. Lett.* **2004**, *85*, 4142.
(26) Gao, P. X.; Lao, C. S.; Ding, Y.; Wang, Z. L. *Adv. Funct. Mater.* **2006**, *16*, 53.
(27) Wang, Z. L.; Kong, X. Y.; Zuo, J. M. *Phys. Rev. Lett.* **2003**, *91*, 185502.
(28) Zhang, X. L.; Kang, Y. S. *Inorg. Chem.* **2006**, *45*, 4186.
(29) Ramgir, N. S.; Late, D. J.; Bhise, A. B.; More, M. A.; Mulla, I. S.; Joag, D. S.; Vijayamohanan, K. *J. Phys. Chem. B* **2006**, *110*, 18236.
(30) Umar, A.; Kim, S. H.; Im, Y. H.; Hahn, Y. B. *Superlattices Microstruct.* **2006**, *39*, 238.
(31) Zeng, H.; Cai, W. P.; Cao, B. Q.; Hu, J. L.; Li, Y.; Liu, P. S. *Appl. Phys. Lett.* **2006**, *88*, 181905.
(32) Pan, H.; Luo, J. Z.; Sun, H.; Feng, Y. P.; Poh, C.; Jing, J. Y. *Nanotechnology* **2006**, *17*, 2963.
(33) Fan, D. H.; Ning, Z. Y.; Jiang, M. F. *Appl. Surf. Sci.* **2005**, *245*, 414.
(34) Ma, J. G.; Liu, Y. C.; Shao, C. L.; Zhang, J. Y.; Lu, Y. M.; Shen, D. Z.; Fan, X. W. *Phys. Rev. B* **2005**, *71*, 125430.
(35) Vanheusden, K.; Warren, W. L.; Seager, C. H.; Tallant, D. R.; Voigt, J. A.; Gnade, B. E. *J. Appl. Phys.* **1996**, *79*, 7983.
(36) Hu, J. Q.; Li, Q.; Wong, N. B.; Lee, C. S.; Lee, S. T. *Chem. Mater.* **2002**, *14*, 1216.
(37) Yao, B. D.; Chan, Y. F.; Wang, N. *Appl. Phys. Lett.* **2002**, *81*, 757.